

# Proximity-induced spin-triplet superconductivity and edge supercurrent in the topological Kagome metal, $K_{1-x}V_3Sb_5$

Yaojia Wang<sup>1</sup>, Shuoying Yang<sup>1</sup>, Pranava K. Sivakumar<sup>1</sup>, Brenden R. Ortiz<sup>2</sup>, Samuel M.L. Teicher<sup>2</sup>, Heng Wu<sup>1,3</sup>, Abhay K. Srivastava<sup>1</sup>, Chirag Garg<sup>1</sup>, Defa Liu<sup>1</sup>, Stuart S. P. Parkin<sup>1</sup>, Eric S. Toberer<sup>4</sup>, Tyrel McQueen<sup>5</sup>, Stephen D. Wilson<sup>2</sup>, Mazhar N. Ali<sup>1\*</sup>

1) Max Planck Institute of Microstructure Physics, Halle, Saxony-Anhalt, Germany, 06108

2) Materials Department, University of California Santa Barbara, Santa Barbara, CA, USA, 93106

3) College of Physics and Optoelectronic Engineering, Shenzhen University, Shenzhen 518060, China

4) Colorado School of Mines, Golden, Colorado, 80401, USA

5) Johns Hopkins University, Baltimore, Maryland, 21218, USA

## Abstract:

**Materials with transition metals in triangular lattices are of great interest for their potential combination of exotic magnetism and electronic topology. Kagome nets, also known as trihexagonal, are of particular importance since the discovery of geometrically frustrated magnetism and massive Dirac fermions in crystals like Herbertsmithite and  $Fe_3Sn_2$ , respectively. Recently,  $KV_3Sb_5$ , was discovered to be a layered, topological metal with a Kagome net of vanadium, and shown to have a giant extrinsic anomalous Hall effect (AHE) related to its triangular lattice. Here, we fabricated Josephson Junctions (JJ) of  $K_{1-x}V_3Sb_5$  and induced superconductivity over extremely long junction lengths (6  $\mu m$ ). Surprisingly, through magnetoresistance and current vs. phase measurements, we observed evidence of both *spin-triplet* supercurrent and spatially localized conducting channels arising from topological edge states. This observation opens the door to studying the interplay of quantum magnetism, strong correlation, and topology as well as facile generation of spin-triplet supercurrent for quantum device applications.**

Magnetic frustration in crystalline materials comes from lattice-caused restrictions of magnetic degrees of freedom which create competing exchange interactions on coupled spins. The classic example of geometrical magnetic frustration is antiferromagnetic (AF) Heisenberg exchange on a triangular net. It is not trivial to simultaneously satisfy the three bonds of a given triangle, giving rise to strong quantum fluctuations, which can facilitate exotic phenomena like spin liquids, spin ices, valence bond solids, etc<sup>1-3</sup>. Similar to the triangular net, the AF Kagome lattice is also known for being strongly frustrated and yielding a classically infinitely degenerate ground state<sup>4,5</sup>.

Following the discovery of high-temperature superconductivity in 1986 by Bednorz and Muller, P.W. Anderson famously proposed a link between magnetic frustration and superconductivity<sup>6</sup>. He predicted the formation of an unconventional superconducting state comprised of disordered *spin-singlet* cooper pairs in the form of resonating bonds. In superconductors, spin-singlet (spin-triplet) superconducting cooper pairs are formed by two electrons with opposite (equal) spin momenta resulting in a net zero (one) spin polarization. From a spin fluctuation perspective, AF correlations in itinerant magnets can allow for spin-triplet pairing<sup>7</sup>. Spin-triplet superconductivity is of great interest both fundamentally and technologically, as a platform for superconducting spintronics and topological Majorana fermions – which are particularly exciting for quantum computing<sup>8-15</sup>.

So far, finding superconductivity in triangular magnets has proven difficult. Many are insulators and attempts at metallizing these systems through chemical doping has had issues of site-

mixing and lattice distortions that result in ordered ground states, imposter states, or spin-glasses<sup>16</sup>. However, recent theoretical work has explored the possibility of topological superconductivity and chiral metallic conduction in doped triangular frustrated magnets in the spin liquid limit<sup>17,18</sup>. So-called “quantum magnets” like  $\text{Fe}_3\text{Sn}_2$ , which has a Kagome net of Fe that is ferromagnetically ordered, have also been predicted to host topological superconductivity due to their flat-band electrons near the Fermi level<sup>19</sup>. However, the experimental exploration of superconductivity in metallic Kagome magnets is still elusive; none have been shown to superconduct intrinsically or have been proximitized, where interfacing the Kagome material with a superconductor can induce weak superconductivity. This requires either thin films or flakes of the Kagome material to be interfaced with superconducting electrodes, most commonly in the form of a Josephson junction; where two superconductors are coupled via a bridge of non-superconducting material. The interference of supercurrents in JJs is the basis of many extremely important technologies including magnetic resonance imaging and quantum computing (Qubits).

Recently, the layered and exfoliatable compound,  $\text{KV}_3\text{Sb}_5$ , was discovered by Ortiz *et al.*<sup>20</sup>, crystallizing in the hexagonal centrosymmetric space group  $\text{P6}/\text{mmm}$  and composed of Kagome layers of Vanadium interleaved with honeycomb layers of Sb and K (Fig. 1A).  $\text{KV}_3\text{Sb}_5$  was found to be paramagnetic at high temperatures with a transition at 80 K that may be related to an electronic density wave order, suggesting partial localization of charge and significant correlation effects<sup>21</sup>. So far, no long- or short-range order was observed down to 250mK and it was suggested that the local moments might be bound into singlets promoting metal-metal bonding<sup>20,22</sup>. Yang *et al.* recently showed that  $\text{K}_{1-x}\text{V}_3\text{Sb}_5$  possessed highly linear electronic bands, giving rise to Dirac quasiparticles and a correspondingly high conductivity<sup>23</sup> as well as, in the same crystals used in this study, an emergent giant skew-scattering anomalous Hall effect that is ascribed to its triangular lattice<sup>23-25</sup>. These samples have potassium deficiency that may be liberating local vanadium moments in the Kagome net giving rise to exotic properties<sup>22</sup>.

Here, we fabricated JJs of  $\text{K}_{1-x}\text{V}_3\text{Sb}_5$  ( $x \sim 0.26 - 0.31$ ) using Nb electrodes, and induced superconductivity through proximity. The Josephson effect is observed in long channels up to 6  $\mu\text{m}$ , and the JJs exhibit a prominent asymmetry and reversion of the magnetoresistance for the up and down magnetic field sweeps in the superconducting state, demonstrating a *spin-polarized* (*i.e.* spin-triplet) supercurrent. Moreover, the  $I_c$  vs phase (through magnetic field control) interference pattern shows a typical Fraunhofer-like pattern for an applied in-plane field, but an anomalous pattern with a *minimum* at zero-field for an applied out-of-plane field. To the best of our knowledge, this has only been seen in  $\text{CrO}_2$ , a ferromagnetic half-metal, which was induced to a spin-triplet superconducting state by proximity as well. Finally, we also detect a non-vanishing, fast oscillation of  $I_c$  with a scalloped peak-profile, indicating the presence of localized conducting states in the edges of the sample. Theoretical analysis of  $\text{KV}_3\text{Sb}_5$ 's band structure also shows the existence of corresponding topological edge states in the (010) plane. This solidifies  $\text{K}_{1-x}\text{V}_3\text{Sb}_5$  as a platform to study the interplay of superconductivity, quantum magnetism, and topology as well as for facile realization of highly stable spin-triplet JJs for quantum information research.

Josephson junctions with different channel lengths were fabricated on  $\text{K}_{1-x}\text{V}_3\text{Sb}_5$  nanoflakes with Nb ( $\sim 40$  nm thick and  $T_c \sim 6$  K) as the superconducting electrodes. The nanoflakes were exfoliated from similar crystals used in the work by Yang *et al.*<sup>23</sup>, which were grown using the same method as previously described by Ortiz *et al.*<sup>20</sup>. Figure 1B shows a schematic structure of a JJ

device and one of the fabricated devices with channel length  $L$  varying from 0.1  $\mu\text{m}$  to 6.05  $\mu\text{m}$  and a constant thickness of  $\sim 45$  nm. Figure 1C shows the  $R$  vs  $T$  curves of both short ( $L = 0.1$   $\mu\text{m}$ ) and intermediate channels ( $L = 1.88$   $\mu\text{m}$ ), measured by the four-probe method to exclude the contact resistance. A sudden drop in resistance can be seen at 0.76 K and 0.68 K, respectively, to the same artifactual residual resistance value arising from lock-in measurement (see discussion in Supplementary materials and Fig. S1). The  $I$  vs  $V$  curves measured at  $\sim 20$  mK confirm the superconducting state at low temperature (inset of Fig. 1C), evidenced by a sudden jump in voltage beyond  $I_c$ . As expected, these two channels have slightly different transition temperatures, corresponding to their junction length. Note that the 1.88  $\mu\text{m}$  junction has a clearly visible increase in resistance just before the onset of superconducting transition; this has also been observed in JJs of ferromagnets like  $\text{CrO}_2$  and Co and is attributed to the accumulation of spin-polarized supercurrent at the interface<sup>26-28</sup>.

The investigation of the length dependence of the proximity effect is shown in Fig. 2. Fig. 2A shows the  $I$  vs  $V$  curves of different channel lengths measured at 20 mK using two probe method; the superconducting transition is observed up to the maximum length fabricated in this study, 6.05  $\mu\text{m}$ . Surprisingly, the extracted critical current,  $I_c$ , (taken from the peak location on  $dI/dI$  vs  $I$  curve) does not decrease with increasing channel length as expected (Fig. 2B red line). This is distinct from a typical JJ with a transparent interface, in which  $I_c$  should monotonically reduce with increasing channel length (fixed thickness and width), due to reduced coupling between the two superconducting electrodes<sup>29,30</sup>. However, in our devices, the contact resistance of the interface is much higher than the sample resistance (*i.e.* not transparent), thus the interface of each channel must be considered. Hence we extracted the  $I_c R_N$  of different JJs, where  $R_N$  is the normal state resistance of the junction. As shown in Fig. 2B (purple line),  $I_c R_N$  varies weakly with channel length, indicating that the  $I_c$  is indeed being dominated by the interface. A similar order of  $I_c$  is also observed in other devices with similar Nb contact (see details in Fig. S2). Importantly, this implies that, for this width and thickness, we have not yet reached a junction length where the proximity effect is intrinsically limited by  $\text{K}_{1-x}\text{V}_3\text{Sb}_5$ .

In addition to the JJs, we also fabricated the  $\text{K}_{1-x}\text{V}_3\text{Sb}_5$  devices with Au contacts to study the intrinsic properties at ultra-low temperatures. Surprisingly, superconductivity was inconsistently observed in some Au devices with  $T_c \sim 0.6$  K-0.65 K and a high  $I_c \sim 13$ -18  $\mu\text{A}$ , but disappeared in others. Electron dispersive x-ray Spectroscopy (EDS) measurements showed different compositions in the superconducting Au-contacted samples compared with the *non*-superconducting Au-contacted samples; the superconducting samples were closer to the ideal 1:3:5 stoichiometry compared to the non-superconducting samples, see details in the Supplementary materials. This indicates that there may be intrinsic superconductivity in  $\text{KV}_3\text{Sb}_5$ , but it is highly dependent on defect/doping. Very recently, stoichiometric  $\text{CsV}_3\text{Sb}_5$  was found to be an intrinsic superconductor at 2.5 K, possibly arising from competing charge density wave instabilities<sup>21</sup>. It is possible that stoichiometric  $\text{KV}_3\text{Sb}_5$  hosts a similar mechanism, but it is disrupted by potassium deficiency. The  $\text{K}_{1-x}\text{V}_3\text{Sb}_5$  samples in our JJs are significantly potassium deficient ( $x = 0.26 - 0.31$ ) compared with the superconducting Au-contacted samples. Also, the superconducting properties of the JJs present a much smaller  $I_c$  (as expected for a JJ) than the superconducting  $\text{KV}_3\text{Sb}_5$  Au-contacted samples, and that  $I_c$  is highly controlled by the interface, strongly indicating that the superconducting properties of the JJs are arising from the proximity effect, not intrinsic superconductivity.

The injection of supercurrent in  $\text{K}_{1-x}\text{V}_3\text{Sb}_5$  Josephson junctions up to several micrometers is

quite unusual. Such long JJs usually occur in materials with very high mobility that allows for long coherence lengths, such as in ultra-pure Cu and Ag<sup>31</sup>. In general, the coherence length  $\xi_N$  can be extracted based on the equation  $\xi_N = \sqrt{\hbar v_F l_e / 6\pi k_B T}$  that is suitable for spin-singlet pairing in non-magnetic materials<sup>32,33</sup> or spin-triplet pairs in a magnetic system<sup>34</sup>. According to this equation and  $\mu = e l_e / \hbar k_F$  ( $\mu \sim 0.2 m^2/Vs$ ,  $k_F \sim 0.032 \text{ \AA}^{-1}$ ,  $v_F \sim 3.77 \times 10^5 m/s$ ,  $T_c \sim 0.78 \text{ K}$ )<sup>23</sup>, the coherence length  $\xi_N$  is extracted to  $\sim 227 \text{ nm}$ , which is much smaller than the observed junction length. Recently, few micrometer Josephson lengths have been observed in topological materials, such as WTe<sub>2</sub>, which the effect is attributed to the localized edge/hinge states<sup>35</sup>. It has also been shown that a long Josephson length can arise when the non-superconducting bridge material in the JJ is *nearly* superconducting itself (i.e. can superconduct with mild doping)<sup>32,36</sup>. Future work is required to elucidate the underlying cause for the long coherence length in K<sub>1-x</sub>V<sub>3</sub>Sb<sub>5</sub>.

The magnetic field dependence of superconductivity in the K<sub>1-x</sub>V<sub>3</sub>Sb<sub>5</sub> JJs is presented in Fig. 3, showing results of the  $6.05 \mu m$  device. When applying the magnetic field (labeled  $B_y$ ) in the sample plane perpendicular to the current direction (labeled  $I_x$ ) at 20 mK, the breaking of superconductivity is observed at an in-plane critical field ( $B_c$ ) of  $\sim 250 \text{ mT}$  (Fig. 3A). In particular, the  $R$  vs  $B$  curve is asymmetric about zero-field for positive and negative field, but that asymmetry reverses for up-sweep (blue line) and down-sweep (red line) of the field, as indicated by the black arrows in Fig. 3A. This property is also observed when applying an out-of-plane magnetic field ( $B_z$  direction). Shown in Fig. 3B, the  $R$  vs  $B$  curves at 20 mK also present a prominent asymmetry and reverse for up-sweep and down-sweep with an out-of-plane  $B_c$  of  $\sim 85 \text{ mT}$ . This flipping property of the  $R$  vs  $B$  curves is observed in all the measured K<sub>1-x</sub>V<sub>3</sub>Sb<sub>5</sub> JJs and channels (see more data in Supplementary materials) for both in-plane and out-of-plane fields. Also visible in Fig. 3B are fast oscillations overlaid on the background of the  $R$  vs  $B$ . Using Fast Fourier Transform analysis, the frequency of fast oscillation is extracted and found to be  $1.9 \text{ mT}^{-1}$ , and is not sensitive to temperature until very near the superconducting transition, as shown in Fig. 3C (see detailed temperature dependence of  $R$  vs  $B$  curves in Fig. S6). This robust fast oscillation is related to the interference of supercurrent and is modulated by the magnetic flux, like a superconducting quantum interference device (SQUID), and its origin is discussed in greater detail below. Similar to the background of the  $R$  vs  $B$  curves, the fast oscillation also reverses for different field sweep directions (Fig. 3B).

$R$  vs  $B$  curve reversion is a typical feature for spin-related transport<sup>37</sup>, and has been observed in magnetic systems breaking time-reversal symmetry (TRS), like ferromagnetic materials with strong magnetization, or even in normal state transport of frustrated Kagome metals (e.g. Pr<sub>2</sub>Ir<sub>2</sub>O<sub>7</sub>) without magnetic dipole order in which TRS is broken by chiral spin texture<sup>38</sup>. So far, there is no evidence of spontaneous TRS breaking in KV<sub>3</sub>Sb<sub>5</sub>, since no long or short-range magnetic order has been observed down to  $0.25 \text{ K}$  (*below* the  $T_c$  of these JJs), nor has hysteresis of the normal state been detected<sup>20,23</sup>. It should be mentioned that our superconducting K<sub>1-x</sub>V<sub>3</sub>Sb<sub>5</sub> devices with Au contacts present normal  $R$  vs  $B$  patterns, *without* reversion (see Fig. S4). The emergence of reversed  $R$  vs  $B$  curves in the superconducting state of the K<sub>1-x</sub>V<sub>3</sub>Sb<sub>5</sub> JJs indicate the presence of a spin-polarized supercurrent. Since Nb is a standard spin-singlet superconductor, the spin-triplet cooper pairs must be formed from the conversion of injected singlet cooper pairs into triplet cooper pairs inside the K<sub>1-x</sub>V<sub>3</sub>Sb<sub>5</sub>.

The proximity effect is a known method to generate spin-triplet Cooper pairs, particularly using heterostructures of conventional superconductors (S) and ferromagnetic (F) metals<sup>39,40</sup>. At the interface of SF, the spin-singlet cooper pair can be converted to the triplet state when there is

breaking of spin-rotation symmetry (allowing the spin-flipping process), which can be achieved using noncollinear, spin inhomogeneous, or spin-spiral magnetizations<sup>39-44</sup>. This has experimentally been realized in JJs of multilayers of different ferromagnets<sup>30,45</sup> (such as the SF'FF''S structure), as well as half-metals (e.g. CrO<sub>2</sub>)<sup>46,47</sup>, ferromagnetic semiconductors (Fe-doped InAs)<sup>34</sup>, or strongly spin-orbit-coupled SF heterostructures<sup>48</sup>. K<sub>1-x</sub>V<sub>3</sub>Sb<sub>5</sub>, does not satisfy any of these conditions, however induced magnetism from the potassium deficiency may result in non-collinear spin structures at the interface that break spin-rotation symmetry, in analogy to the SF'FF''S junctions<sup>39,40</sup>, but in a single material rather than a multi-layer stack. Since the field dependence of the resistance of the JJ is controlled by the phase modulation of the Josephson current and, for spin-triplet pairing, that phase modulation is also dependent on local spin structures<sup>49</sup> at the interface; opposite modulation of those spin structures by switching field sweeping directions will result in the reversed  $R$  vs  $B$  curves.

The phase modulations of the supercurrent are further studied in the K<sub>1-x</sub>V<sub>3</sub>Sb<sub>5</sub> JJs by applying both in-plane and out-of-plane magnetic fields. In a JJ, the  $I_c$  is related to the phase difference between the two superconducting electrodes that is modulated by the magnetic flux through the junction. The  $dV/dI$  versus  $I$  was measured at different magnetic fields with fixed field sweeping directions. Figs. 4A and 4B are the color maps of  $dV/dI$  vs  $I$  and  $B$  for in-plane field and out-of-plane field respectively, measured by down-sweep of the field for the 6.05  $\mu\text{m}$  JJ (see Fig. S7 for up-sweep spectrum). Note that there are two sets of interference patterns of critical currents (bright lines) on the color maps, which may be indicative of distinct superconducting channels in the K<sub>1-x</sub>V<sub>3</sub>Sb<sub>5</sub> JJ (see detailed discussion in Supplementary materials). However, since the outside pattern sustains to higher field than the inside pattern and dominates the primary interference features, we focus on the outside pattern. When applying the in-plane magnetic field, with  $B_y \perp I_x$ , the main interference pattern of  $I_c$  vs  $B$  shows a prominent peak at zero field and the oscillation of  $I_c$  decays like  $1/B$  with increasing field, as is expected of a standard Fraunhofer-like  $I_c$  vs  $B$  pattern of a JJ. This is another confirmation that Josephson coupling is achieved in these devices. However, when applying an out-of-plane ( $B_z$ ) magnetic field (Fig. 4B), the critical current shows an anomalous suppression near zero field, resulting in a *minimum* instead of a peak, at the center of interference pattern. Under very weak magnetic field (either up or down), the  $I_c$  is actually enhanced relative to zero-field. Additionally, a fast, SQUID-like oscillation is clearly visible on top of the primary background.

A minimum of  $I_c$  at zero-field of a JJ interference pattern for a single material has rarely been observed. JJs of non-magnetic and most ferromagnetic materials generally have a standard single-slit Fraunhofer interference pattern with a central maximum (shifted by internal magnetization). One example of the zero-field minimum was observed in the spin-triplet JJ of the ferromagnetic half-metal, CrO<sub>2</sub>, which was speculated to be caused by a finite magnetization induced flux density offset<sup>46</sup>, but a clear understanding of the physical mechanism is still needed. In K<sub>1-x</sub>V<sub>3</sub>Sb<sub>5</sub> JJs, the  $I_c$  is strongly suppressed by the out-of-plane field and its maximum value upon down-sweep ( $\sim 0.32 \mu\text{A}$ , Fig. 4B) is only half of the zero-field cooled critical current ( $\sim 0.63 \mu\text{A}$ , see red line of Fig. 2A). By contrast, the in-plane field has a weaker effect on the maximum of  $I_c$  ( $\sim 0.55 \mu\text{A}$  on Fig. 4A). This anisotropic field dependence of  $I_c$  may be evidence of the in-plane stability of local spin structures, which is consistent with the theoretical calculation of in-plane magnetism in K<sub>1-x</sub>V<sub>3</sub>Sb<sub>5</sub><sup>20</sup>. Under out-of-plane field, depending on the anisotropy strength of the magnetic coupling, out-of-plane canting will change the interfacial spin structure, and correspondingly influence the

transparency of the interface to supercurrent injection from the Nb. Detailed future theoretical and experimental work are required to fully understand this observation. Note that the superconducting Au-contacted  $K_{1-x}V_3Sb_5$  devices present typical  $I_c$  vs  $B$  dependencies (see Fig. S4), *i.e.* a monotonically decreasing  $I_c$  with increasing  $B$ , without suppression at zero field, indicating that the anisotropic and suppressed field dependencies of  $I_c$  in the JJs are related to the generation of spin-triplet Cooper pairs in the proximitized  $K_{1-x}V_3Sb_5$ .

Finally, we focus on the spatial properties of the supercurrent and the fast, SQUID-like oscillation of  $I_c$  in the Figure 4. The  $I_c$  is modulated by the magnetic flux in units of the flux quantum  $\Phi_0$ , so for the in-plane magnetic field the Fraunhofer-like pattern (period of  $\Delta B \sim 100$  mT) corresponds to an effective superconducting thickness of  $t_{\text{eff}} \approx 3.4$  nm, according to  $\Phi_0 = \Delta B * L * t_{\text{eff}}$  ( $L \approx 6.05$   $\mu\text{m}$ ). Inverse Fourier transforms of the in-plane interference pattern (see Fig. S8) to recover the current density profile also shows that supercurrent is uniformly distributed through the top  $\sim 5$  nm of the flake, which is in good agreement with  $t_{\text{eff}}$ . These results imply that only a thin layer on the top of the flake is being proximitized; the superconducting order is not extending deeply along the  $c$ -axis across the layers, and is dramatically longer in the  $ab$ -plane. This thin proximitized layer is reasonable for  $K_{1-x}V_3Sb_5$  due to its layered structure, which is expected to be electronically anisotropic ( $c$  axis vs the  $ab$ -plane) like its sister material  $CsV_3Sb_5$  ( $\sim 600\times$  anisotropy)<sup>21</sup>. This results in a shortened coherence length along the  $c$ -axis, similar to other layered materials like  $WTe_2$ <sup>33</sup>. The interference pattern from the out-of-plane magnetic field, however, with fast oscillations on top of the background is not a typical Fraunhofer pattern. The fast oscillation maintains a period of  $\Delta B \sim 0.5$  mT that is consistent with the frequency of the oscillation on the  $R$  vs  $B$  curves and corresponds to an effective flux-penetration area of  $S_{\text{eff}} \sim 4.13$   $\mu\text{m}^2$  calculated from  $\Phi_0 = \Delta B * S_{\text{eff}}$ . This is smaller than the crystal area ( $S = L * W \approx 12$   $\mu\text{m}^2$ ), which and may be caused by partial penetration of the flux, like was seen with  $MoTe_2$ <sup>50</sup>. The most important feature of the fast oscillation is that it is non-vanishing and maintains to higher field than the main interference pattern, as shown in Fig. 4B. This long-lived, fast oscillation cannot be induced by the bulk Josephson current. Moreover, it presents a scalloped peak profile (Fig. 4C) with clear excitation branches trailing from the scalloped boundary. This scalloped profile of a non-vanishing fast mode is an important signature of multiple non-bulk, spatially localized states (*i.e.* not uniformly distributed supercurrent). In this case, for an enclosed area bounded by the edges, the requirement of flux quantization results in a sawtooth profile of the edge Fermi velocity, which contributes to the scalloped profile. The same scalloped shape and non-vanishing SQUID-like oscillation (with a similar device geometry) was recently reported in the higher order semimetal  $MoTe_2$ <sup>50</sup>.

To examine the possible origin of this edge-localized supercurrent, we performed density functional theory (DFT) calculations of the electronic band structure of  $KV_3Sb_5$ . Previous work on the isostructural, isoelectronic compound  $CsV_3Sb_5$  had predicted a number of surface states, including  $\mathbb{Z}_2$ -protected topological surface Dirac crossings just above the Fermi level<sup>21</sup>. The band structure and surface states of  $KV_3Sb_5$  are calculated to be virtually identical, including  $\mathbb{Z}_2$  states. Fig. 4D shows the spectral density of bulk (upper panel) and surface states (lower panel) on the (100)/(010) planes ( $ac/bc$  planes), including states propagating along the [001] and [100]/[010] directions. While the large number of surface states prevents us from attributing the surface conductivity to a single surface band, our calculations show that relevant topological surface states (note the X-M line) exist within range of our chemical composition. See the supplementary for further discussion. Importantly, the surface states in the  $ab$ -plane were not detected in our JJs when

applying in-plane field along the  $y$ -axis, likely because only the top layers of the  $K_{1-x}V_3Sb_5$  samples were proximitized; coupling between the top and bottom surface states to result in the SQUID-like pattern was not possible, in analogy to what was seen with the hinge-states in  $Al_2O_3$  back-filled  $WTe_2$  devices<sup>51</sup>. Future work applying in-plane field on ultra-thin  $K_{1-x}V_3Sb_5$  JJs may be able to probe the  $ab$ -surface state coupling as well.

In summary, we fabricated JJs of the topological Kagome metal,  $K_{1-x}V_3Sb_5$ , and discovered 1.) extremely long Josephson coupling of at least  $6\ \mu m$ , 2.) multiple pieces of evidence of spin-triplet supercurrent (asymmetry and reversion of  $R$  vs  $B$  as well as a zero-field minimum in the  $I_c$  vs  $B$  pattern) and 3.) the interference pattern signature of the predicted topological edge states in  $K_{1-x}V_3Sb_5$ . This is the first time a metallic frustrated magnet candidate has been coaxed into superconducting (that also happens to host multiple topological surface states) and opens the door for exploring the combination of superconductivity with quantum magnetism and topology. There is a variety of future theoretical and experimental work in fully understanding the effect of non-stoichiometry, the spin-triplet conversion mechanism, its spin related properties, and relation to unconventional and topological superconductivity, as well as the nature of the topological surface and edge states. Technologically,  $K_{1-x}V_3Sb_5$  is a promising material for creating highly stable spin-triplet JJs for quantum computing and sensor applications. It will also be interesting to explore the possible topological and/or chiral superconductivity of  $K_{1-x}V_3Sb_5$  in future works.

## References:

1. M. R. Norman, Colloquium: Herbertsmithite and the search for the quantum spin liquid. *Rev. Mod. Phys.* **88**, 041002 (2016).
2. S. T. Bramwell, M. J. P. Gingras, Spin ice state in frustrated magnetic pyrochlore materials. *Science*. **294**, 1495–1501 (2001).
3. L. Balents, Spin liquids in frustrated magnets. *Nature*. **464**, 199–208 (2010).
4. G. Xu, C. Broholm, D. H. Reich, M. A. Adams, Triplet waves in a quantum spin liquid. *Phys. Rev. Lett.* **84**, 4465–4468 (2000).
5. P. Fazekas, P. W. Anderson, On the ground state properties of the anisotropic triangular antiferromagnet. *Philos. Mag.* **30**, 423–440 (1974).
6. P. W. Anderson, The Resonating Valence Bond State in  $\text{La}_2\text{CuO}_4$  and Superconductivity. *Science*. **235**, 1196–1198 (1986).
7. S. Li, P. Dai, Superconductivity and spin fluctuations. *Front. Phys.* **6**, 429–439 (2011).
8. R. M. Lutchyn, E. P. A. M. Bakkers, L. P. Kouwenhoven, P. Krogstrup, C. M. Marcus, Y. Oreg, Majorana zero modes in superconductor-semiconductor heterostructures. *Nat. Rev. Mater.* **3**, 52–68 (2018).
9. A. Pustogow, Y. Luo, A. Chronister, Y. S. Su, D. A. Sokolov, F. Jerzembeck, A. P. Mackenzie, C. W. Hicks, N. Kikugawa, S. Raghu, E. D. Bauer, S. E. Brown, Constraints on the superconducting order parameter in  $\text{Sr}_2\text{RuO}_4$  from oxygen-17 nuclear magnetic resonance. *Nature*. **574**, 72–75 (2019).
10. K. Matano, M. Kriener, K. Segawa, Y. Ando, G. Q. Zheng, Spin-rotation symmetry breaking in the superconducting state of  $\text{Cu}_x\text{Bi}_2\text{Se}_3$ . *Nat. Phys.* **12**, 852–854 (2016).
11. P. Zhang, K. Yaji, T. Hashimoto, Y. Ota, T. Kondo, K. Okazaki, Z. Wang, J. Wen, G. D. Gu, H. Ding, S. Shin, Observation of topological superconductivity on the surface of an iron-based superconductor. *Science*. **360**, 182–186 (2018).
12. L. Jiao, S. Howard, S. Ran, Z. Wang, J. O. Rodriguez, M. Sgrist, Z. Wang, N. P. Butch, V. Madhavan, Chiral superconductivity in heavy-fermion metal  $\text{UTe}_2$ . *Nature*. **579**, 523–527 (2020).
13. S. Ran, C. Eckberg, Q. P. Ding, Y. Furukawa, T. Metz, S. R. Saha, I. L. Liu, M. Zic, H. Kim, J. Paglione, N. P. Butch, Nearly ferromagnetic spin-triplet superconductivity. *Science*. **365**, 684–687 (2019).
14. N. T. Huy, A. Gasparini, D. E. De Nijs, Y. Huang, J. C. P. Klaasse, T. Gortenmulder, A. De Visser, A. Hamann, T. Görlach, H. V. Löhneysen, Superconductivity on the border of weak itinerant ferromagnetism in  $\text{UGe}_2$ . *Phys. Rev. Lett.* **99**, 067006 (2007).
15. G. R. Stewart, Z. Fisk, J. O. Willis, J. L. Smith, Possibility of coexistence of bulk superconductivity and spin fluctuations in  $\text{UPt}_3$ . *Phys. Rev. Lett.* **52**, 679–682 (1984).
16. R. Zhong, S. Guo, G. Xu, Z. Xu, R. J. Cava, Strong quantum fluctuations in a quantum spin liquid candidate with a Co-based triangular lattice. *Proc. Natl. Acad. Sci. U. S. A.* **116**, 14505–14510 (2019).
17. X. Song, A. Vishwanath, Y. Zhang, Doping the chiral spin liquid - topological superconductor or chiral metal? <https://arxiv.org/pdf/2011.10044> (2020).
18. Y. F. Jiang, H. C. Jiang, Topological Superconductivity in the Doped Chiral Spin Liquid on the Triangular Lattice. *Phys. Rev. Lett.* **125**, 157002 (2020).
19. S. Baidya, A. V. Mallik, S. Bhattacharjee, T. Saha-Dasgupta, Interplay of Magnetism and Topological Superconductivity in Bilayer Kagome Metals. *Phys. Rev. Lett.* **125**, 26401 (2020).



20. B. R. Ortiz, L. C. Gomes, J. R. Morey, M. Winiarski, M. Bordelon, J. S. Mangum, I. W. H. Oswald, J. A. Rodriguez-Rivera, J. R. Neilson, S. D. Wilson, E. Ertekin, T. M. McQueen, E. S. Toberer, New kagome prototype materials: Discovery of  $\text{KV}_3\text{Sb}_5$ ,  $\text{RbV}_3\text{Sb}_5$ , and  $\text{CsV}_3\text{Sb}_5$ . *Phys. Rev. Mater.* **3**, 094407 (2019).
21. B. R. Ortiz, S. M. L. Teicher, Y. Hu, J. L. Zuo, P. M. Sarte, E. C. Schueller, A. M. M. Abeykoon, M. J. Krogstad, S. Rosenkranz, R. Osborn, R. Seshadri, L. Balents, J. He, S. D. Wilson,  $\text{CsV}_3\text{Sb}_5$ : a  $\text{Z}_2$  topological kagome metal with a superconducting ground state. <https://arxiv.org/abs/2011.06745> (2020)
22. E. M. Kenney, B. R. Ortiz, C. Wang, S. D. Wilson, M. J. Graf, Absence of local moments in the kagome metal  $\text{KV}_3\text{Sb}_5$  as determined by muon spin spectroscopy. <https://arxiv.org/abs/2012.04737> (2020).
23. S. Y. Yang, Y. Wang, B. R. Ortiz, D. Liu, J. Gayles, E. Derunova, R. Gonzalez-Hernandez, L. Šmejkal, Y. Chen, S. S. P. Parkin, S. D. Wilson, E. S. Toberer, T. McQueen, M. N. Ali, Giant, unconventional anomalous Hall effect in the metallic frustrated magnet candidate,  $\text{KV}_3\text{Sb}_5$ . *Sci. Adv.* **6**, eabb6003 (2020).
24. H. Ishizuka, N. Nagaosa, Theory of giant skew scattering by spin cluster. <https://arxiv.org/abs/1906.06501> (2019)
25. H. Ishizuka, N. Nagaosa, Spin chirality induced skew scattering and anomalous hall effect in chiral magnets. *Sci. Adv.* **4**, eaap9962 (2018).
26. A. Singh, S. Voltan, K. Lahabi, J. Aarts, Colossal proximity effect in a superconducting triplet spin valve based on the half-metallic ferromagnet  $\text{CrO}_2$ . *Phys. Rev. X* **5**, 021019 (2015).
27. J. Wang, M. Singh, M. Tian, N. Kumar, B. Liu, C. Shi, J. K. Jain, N. Samarth, T. E. Mallouk, M. H. W. Chan, Interplay between superconductivity and ferromagnetism in crystalline nanowires. *Nat. Phys.* **6**, 389–394 (2010).
28. S. Voltan, A. Singh, J. Aarts, Triplet generation and upper critical field in superconducting spin valves based on  $\text{CrO}_2$ . *Phys. Rev. B* **94**, 054503 (2016).
29. P. Dubos, H. Courtois, B. Pannetier, F. K. Wilhelm, A. D. Zaikin, G. Schön, Josephson critical current in a long mesoscopic S-N-S junction. *Phys. Rev. B* **63**, 064502 (2001).
30. T. S. Khaire, M. A. Khasawneh, W. P. Pratt, N. O. Birge, Observation of spin-triplet superconductivity in co-based josephson junctions. *Phys. Rev. Lett.* **104**, 137002 (2010).
31. H. Courtois, P. Gandit, B. Pannetier, Proximity-induced superconductivity in a narrow metallic wire. *Phys. Rev. B* **52**, 1162–1166 (1995).
32. I. Bozovic, G. Logvenov, M. A. J. Verhoeven, P. Caputo, E. Goldobin, M. R. Beasley, Giant proximity effect in cuprate superconductors. *Phys. Rev. Lett.* **93**, 157002 (2004).
33. Q. Li, C. He, Y. Wang, E. Liu, M. Wang, Y. Wang, J. Zeng, Z. Ma, T. Cao, C. Yi, N. Wang, K. Watanabe, T. Taniguchi, L. Shao, Y. Shi, X. Chen, S. J. Liang, Q. H. Wang, F. Miao, Proximity-Induced Superconductivity with Subgap Anomaly in Type II Weyl Semi-Metal  $\text{WTe}_2$ . *Nano Lett.* **18**, 7962–7968 (2018).
34. T. Nakamura, L. D. Anh, Y. Hashimoto, S. Ohya, M. Tanaka, S. Katsumoto, Evidence for Spin-Triplet Electron Pairing in the Proximity-Induced Superconducting State of an Fe-Doped InAs Semiconductor. *Phys. Rev. Lett.* **122**, 107001 (2019).
35. A. Kononov, A. Kononov, G. Abulizi, K. Qu, J. Yan, J. Yan, D. Mandrus, D. Mandrus, K. Watanabe, T. Taniguchi, C. Schönenberger, C. Schönenberger, One-Dimensional Edge Transport in Few-Layer  $\text{WTe}_2$ . *Nano Lett.* **20**, 4228–4233 (2020).

36. L. Covaci, F. Marsiglio, Proximity effect and Josephson current in clean strong/weak/strong superconducting trilayers. *Phys. Rev. B* **73**, 014503 (2006).
37. N. Banerjee, J. W. A. Robinson, M. G. Blamire, Reversible control of spin-polarized supercurrents in ferromagnetic Josephson junctions. *Nat. Commun.* **5**, 4771 (2014).
38. Y. MacHida, S. Nakatsuji, S. Onoda, T. Tayama, T. Sakakibara, Time-reversal symmetry breaking and spontaneous Hall effect without magnetic dipole order. *Nature*. **463**, 210–213 (2010).
39. M. Eschrig, Spin-polarized supercurrents for spintronics. *Phys. Today*. **64**, 43–49 (2011).
40. N. O. Birge, Spin-triplet supercurrents in Josephson junctions containing strong ferromagnetic materials. *Philos. Trans. R. Soc. A* **376**, 20150150 (2018).
41. W. Han, S. Maekawa, X. C. Xie, Spin current as a probe of quantum materials. *Nat. Mater.* **19**, 139–152 (2020).
42. J. Linder, J. W. A. Robinson, Superconducting spintronics. *Nat. Phys.* **11**, 307–315 (2015).
43. M. Eschrig, T. Löfwander, Triplet supercurrents in clean and disordered half-metallic ferromagnets. *Nat. Phys.* **4**, 138–143 (2008).
44. M. Houzet, A. I. Buzdin, Long range triplet Josephson effect through a ferromagnetic trilayer. *Phys. Rev. B* **76**, 060504 (2007).
45. J. W. A. Robinson, J. D. S. Witt, M. G. Blamire, Controlled injection of spin-triplet supercurrents into a strong ferromagnet. *Science*. **329**, 59–61 (2010).
46. R. S. Keizer, S. T. B. Goennenwein, T. M. Klapwijk, G. Miao, G. Xiao, A. Gupta, A spin triplet supercurrent through the half-metallic ferromagnet CrO<sub>2</sub>. *Nature*. **439**, 825–827 (2006).
47. C. Visani, Z. Sefrioui, J. Tornos, C. Leon, J. Briatico, M. Bibes, A. Barthélémy, J. Santamaría, J. E. Villegas, Equal-spin Andreev reflection and long-range coherent transport in high-temperature superconductor/half-metallic ferromagnet junctions. *Nat. Phys.* **8**, 539–543 (2012).
48. D. Breunig, P. Burset, B. Trauzettel, Creation of Spin-Triplet Cooper Pairs in the Absence of Magnetic Ordering. *Phys. Rev. Lett.* **120**, 37701 (2018).
49. A. Pal, Z. H. Barber, J. W. A. Robinson, M. G. Blamire, Pure second harmonic current-phase relation in spin-filter Josephson junctions. *Nat. Commun.* **5**, 3340 (2014).
50. W. Wang, S. Kim, M. Liu, F. A. Cevallos, R. J. Cava, N. P. Ong, Evidence for an edge supercurrent in the Weyl superconductor MoTe<sub>2</sub>. *Science*. **368**, 534–537 (2020).
51. Y. Bin Choi, Y. Xie, C. Z. Chen, J. Park, S. B. Song, J. Yoon, B. J. Kim, T. Taniguchi, K. Watanabe, J. Kim, K. C. Fong, M. N. Ali, K. T. Law, G. H. Lee, Evidence of higher-order topology in multilayer WTe<sub>2</sub> from Josephson coupling through anisotropic hinge states. *Nat. Mater.* **19**, 974–979 (2020).

## Acknowledgments:

We thank Fang Gao and Jae-Chun Jeon for the support during device fabrication, and thank Gil-Ho Lee and Vic K. T. Law and for valuable discussions. **Funding:** M.N.A acknowledges that this research was principally supported by the Alexander von Humboldt Foundation Sofia Kovalevskaja Award, the German Federal Ministry of Education and Research's MINERVA ARCHES Award, and the Max Planck Society. S. D.W., B. R. O., and S. M. L. T. acknowledge support from the University of California Santa Barbara Quantum Foundry, funded by the National Science Foundation (NSF DMR-1906325). Research reported here also made use of shared facilities of the UCSB MRSEC (NSF DMR-1720256). B. R. O. also acknowledges support from the California NanoSystems Institute through the Elings fellowship

program. S.M. L. T. has been supported by the National Science Foundation Graduate Research Fellowship Program under Grant No. DGE-1650114. Any opinions, findings, and conclusions or recommendations expressed in this material are those of the authors and do not necessarily reflect the views of the National Science Foundation. D.L. acknowledges support from the Alexander von Humboldt Foundation. S.S.P.P. acknowledges the European Research Council (ERC) under the European Union's Horizon 2020 research and innovation programme (grant agreement no. 670166), Deutsche Forschungsgemeinschaft (DFG, German Research Foundation)—project number 314790414, and Alexander von Humboldt Foundation in the framework of the Alexander von Humboldt Professorship endowed by the Federal Ministry of Education and Research. T.M. acknowledges the David and Lucile Packard Foundation and the Johns Hopkins University Catalyst Award. E.S.T. acknowledges the NSF award 1555340.

**Author contributions:** Y.W. and M.N.A. conceived and designed the study. B.R.O. grew the samples. Y.W. and S.-Y.Y. fabricated the devices. Y.W., P.K.S. and S.-Y.Y. performed the transport measurement. Y.W, H.W, S.-Y. Y., C. G. and D.L carried out the data analysis. S.M.L.T. carried out DFT calculations and theoretical analysis. A.K.S. performed the EDX measurements. E.S.T., T.M., S.D.W., and M.N.A are the Principal Investigators. All authors contributed to the preparation of manuscript.

**Competing interests:** The authors declare that they have no competing interests.

**Data and materials availability:** All data needed to evaluate the conclusions in the paper are present in the paper and/or the Supplementary Materials. Additional data related to this paper may be requested from the authors.

**Corresponding author email:** maz@berkeley.edu

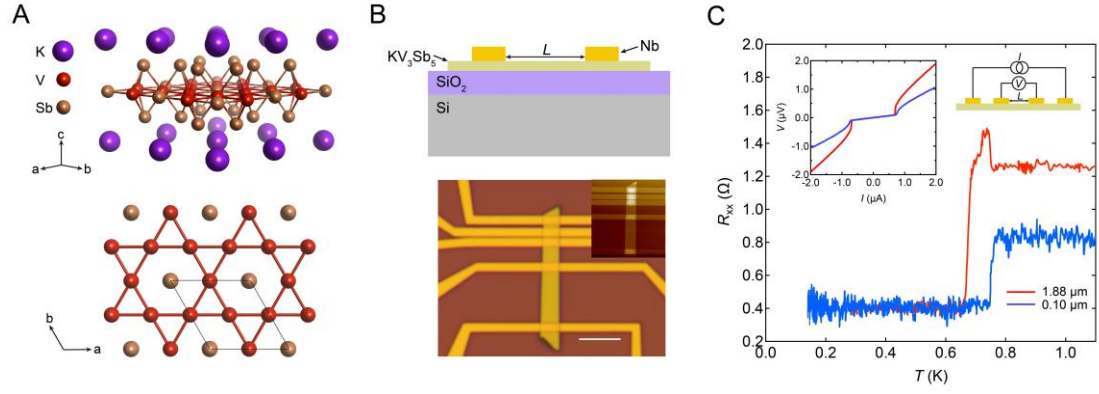


**Fig. 1. Crystal structure and Josephson junction of  $KV_3Sb_5$ .** (A). Top: Crystal structure of  $KV_3Sb_5$ , Bottom: Projection along  $c$ -axis showing the Kagome net of Vanadiums. (B). The top panel is side-view schematic of  $K_{1-x}V_3Sb_5$  Josephson junction, the bottom panel is the optical and AFM (inset) image of one fabricated JJ device of  $K_{1-x}V_3Sb_5$  thin flake ( $\sim 45$  nm), the scale bar is  $5\ \mu\text{m}$ . (C). Superconducting transition of Josephson junction measured by four-probe method. The insets are measurement circuit and typical voltage versus current curves measured at 20 mK.

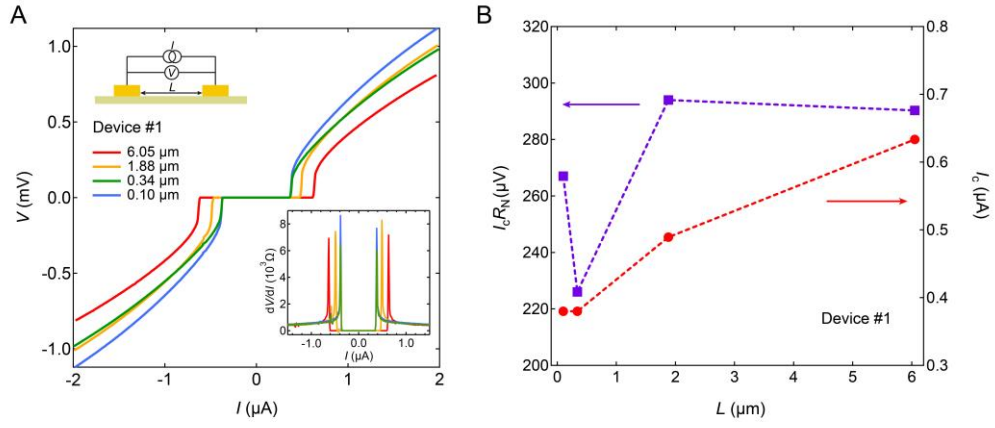


**Fig. 2. Length dependence of Josephson current.** (A). Voltage versus current ( $V$ - $I$ ) curves for different channel lengths measured by two-probe method at 20 mK. The insets are corresponding differential resistance and schematic of measurement circuit. (B). Length dependent critical currents  $I_c$  and  $I_c R_N$  extracted from the  $V$ - $I$  curves in (A).

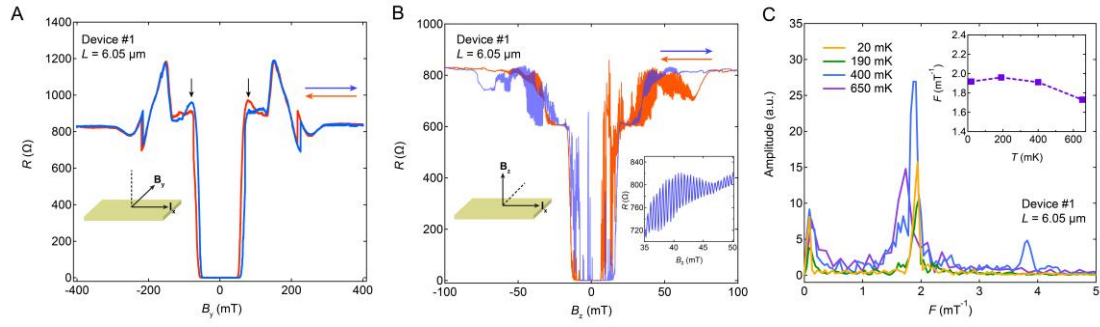


**Fig. 3. Magnetic field dependent resistance of Josephson junction with  $L=6.05 \mu\text{m}$ .** (A).  $R$  vs  $B$  with magnetic field applied in-plane but orthogonal to the current. Red (blue) line and arrows denote field down (up) sweeping. The two black arrows point out the reversion of resistance for different sweep directions. The inset denotes magnetic field and current directions. (B).  $R$  vs  $B$  of the same device with magnetic field applied out of plane and orthogonal to the current. The left inset denotes magnetic field and current directions and the right inset is the enlarged plot of fast oscillation. (C). Fast-Fourier transform (FFT) of fast oscillation in (B) at different temperatures, the inset is temperature dependent oscillation frequency obtained in (C).

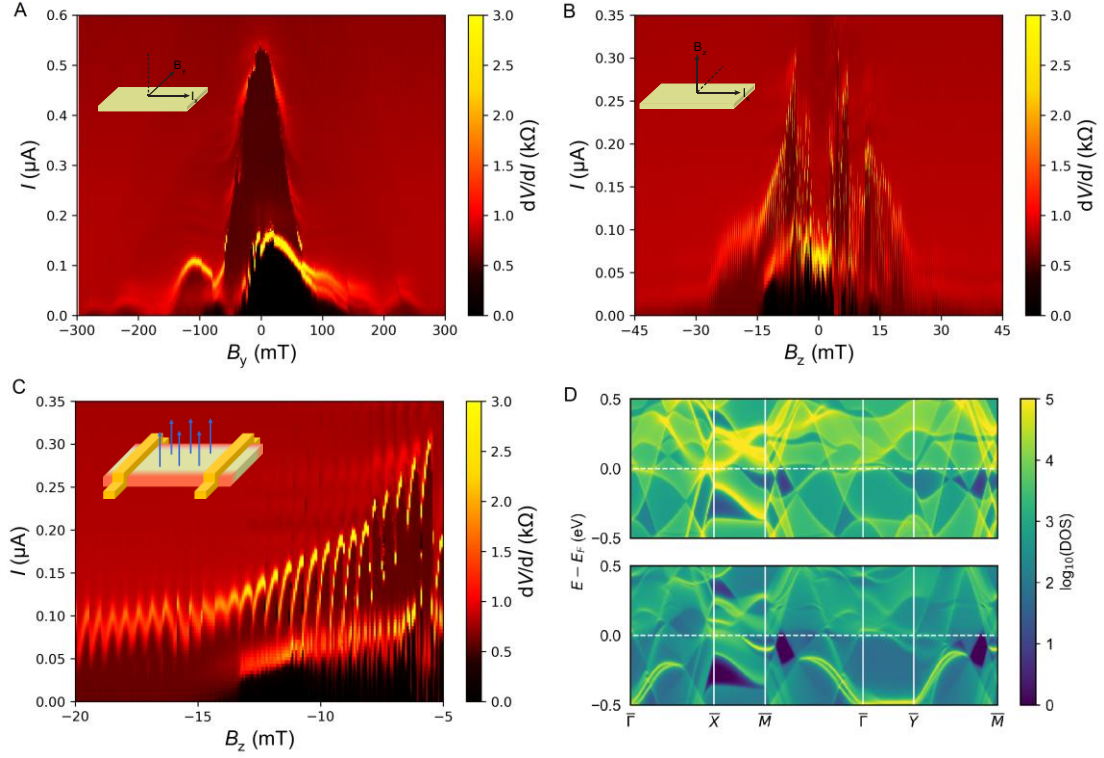


**Fig .4. Interference patterns and localized Josephson current.** (A) and (B) are color maps of  $dV/dI$  versus current and magnetic field measured in Device #1 at 20 mK with applying in-plane magnetic field and out-of-plane magnetic field, respectively. The field is changing from positive to negative during the measurement. The insets denote magnetic field and current directions. (C). The enlarged plots of the fast oscillation in (B) for applying out-of-plane field. The inset is a schematic of the edge supercurrent in the JJ, the edges are indicated by red color. (D). Top: Bulk spectral density of states for  $KV_3Sb_5$  on the (010/100) surfaces. Bottom: Surface spectral density of states for the (010/100) surfaces. Several bright bands are present in the bottom panel but not the top panel; these are the surface states.